Implementation and Observation of EKV 2.6 Model

Hanbin Hu No. 1132109003
School of Microelectronics, Shanghai Jiao Tong University, Shanghai 200240, China
Email: huhanbinnew@hotmail.com

***Abstract*—Low power low voltage design is increasingly popular in analog circuit design in recent years. EKV model and g_m/I_D methodology focused on this sort of design is verified in the past 20 years. This article illustrates the basic EKV model and explain several secondary effects considered in EKV 2.6 model. A CAD tool with GUI implemented with an engine simulating EKV 2.6 model is given. Several simulation results are given and discussed, showing that current EKV model realized still need to consider more effects to cater the requirement of g_m/I_D methodology.**

***Index Terms*—EKV 2.6, transconductance efficiency, inversion coefficient, g_m/I_D methodology.**

I. Introduction

Low power low voltage design is increasingly popular in analog circuit design in the past decade, due to the reduction in the minimum dimension led by the development of fabrication process. This trend requires MOS transistor to work in moderate inversion, or even weak inversion. Analog circuit design largely depends on the characteristics of device and profound design insights into circuit performance. However, the traditional square-law MOS model [1] doesn't describe the accurate behaviour of transistors in the weak or moderate inversion, which hinders the analysis and optimization for circuit design and lowers design efficiency.

Charge Sheet Model (CSM) is put forward so at to model the operation of MOS transistor in all working region [2], [3], while the model is too complicated to allow hand-analysis. An analytical MOS transistor model valid in all regions of operation is then proposed by Enz, Krummenacher and Vittoz (EKV) simplifying CSM model. [4]. This model makes hand-design feasible and employ a single equation applicable to all operation regions of MOS transistor, which provides a powerful tool for circuit designers to size transistors in weak or moderate inversion.

G_m/I_D methodology based on EKV model is one of the most popular design methodology focused on low power low voltage analog circuit design. [5], [6] A CAD tool is also programmed in 2003 to provide support for this method. [7] This work reviews the basic EKV model, and introduce EKV 2.6 model, [8] and design a CAD tool to obviously present the impact of transistor dimension and voltage bias on MOS performance.

The report is organized as follows. Section II describes the fundamental EKV model and explains some second-order effects considered in EKV 2.6 model. In Section III, a software with Graphical User Interface (GUI) integrated with a EKV 2.6 model is illustrated. Several simulation results based on different simulators are presented and discussed in Section IV. Section V concludes the report. Some equation derivation is summarized in the Appendix.

II. EKV 2.6 Model Introduction

A. Review on Fundamental EKV Model

Compared to CSM model, EKV model linearize the surface potential of the MOS transistor and solve the Boltzmann distribution equation through Taylor approximation, employing pinch-off voltage V_P and normalized mobile charge density q. After the derivation, one basic equation for EKV is presented as follows.

$$\begin{cases} i = q^2 + q \\ V_P - V(x) = V_T [2q + \ln q] \end{cases} \tag{1}$$

In Equation 1, i represents the inversion level of transistor, and $V(x)$ is the voltage along the channel, besides that, V_T stands for the thermal voltage. Particularly, when $V(x)$ equals the source voltage or drain voltage of transistor, the corresponding i indicate the inversion level for forward current i_f and reverse one i_r, and the difference between these two value is known as inversion coefficient IC. To obtain the analytical form for drain current, the formula below is required.

$$\begin{cases} I_{DS} = I_N (i_f - i_r) = I_N \cdot IC \\ I_N = 2nV_T^2\beta = 2nV_T^2\mu C_{ox}\frac{W}{L} = I_0\frac{W}{L} \end{cases} \tag{2}$$

I_N here is normalized current, n is the slope factor induced by the slight change of surface potential, μ stands for the mobility of carrier and C_{ox} is unit capacitance of gate oxide layer. I_0 is the drain current with unit inversion coefficient and the same size of width and length, only depending on process. According to the equation above, we can solve the equation for g_m/I_D as follows.

$$\frac{g_m}{I_D} = \frac{1}{I_D}\frac{\partial I_D}{\partial V_G} = \frac{\partial \ln I_D}{\partial V_G} = \frac{\partial \ln\left\{\frac{I_D}{\left(\frac{W}{L}\right)}\right\}}{\partial V_G} \tag{3}$$

From the equation above, we can see the ratio of transconductance g_m and drain current I_D is related to the sizing of MOS transistor. Moreover, g_m/I_D vs. IC curve is a stable curve only determined by the process parameter, which implies the convenience of g_m/I_D guiding the sizing of MOS transistor. [5], [9]

B. Second-Order Effect Considered in EKV 2.6

The EKV 2.6 model includes the second-order effect including channel length modulation (CLM), velocity saturation, short and narrow channel source and drain charge-sharing, reverse short channel effect (RSCE) and mobility effects due to vertical fields. The following will explain the physical mechanism for each effects. Only NMOS is considered here.

1) Channel length modulation: CLM is one of the most common second-order effect in MOS transistor, reflected on β. Assuming the transistor works in strong inversion, as the drain voltage increases, the potential between drain and bulk increases, meanwhile leading to lateral extension of the depletion region to channel. At some critical point, the channel pinch-off at drain terminal. If the drain voltage keep increasing, the effective channel length will be minimized. Therefore, the effective channel length L_{eff} should be modified as $L - \Delta L$, shown in Fig. 1. [1] ΔL is mainly determined by V_{ds} and process technology.

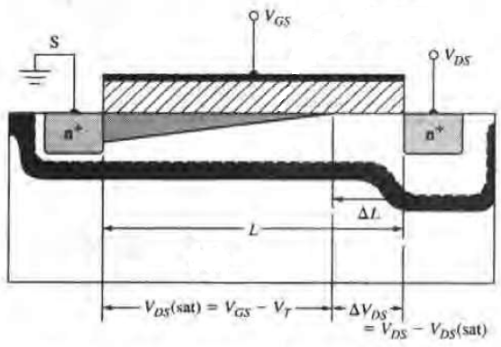

Fig. 1. Channel length modulation

2) Velocity saturation: In the traditional long-channel MOSFET analysis, mobility is assumed a constant, which means the drift velocity will arbitrary large when the electric field is strong enough. Actually, due to scattering effects (collisions suffered by the carrier), the velocity of the carriers tends to saturate at a critical value of electric field. [10] The saturation velocity v_{sat} is also considered in the effect channel length L_{eff} of EKV 2.6, by telling the starting point of electric field intensity to saturate E_{sat}.

3) Short and narrow channel source and drain charge-sharing: When the typical size is short, some modification of threshold voltage need to be considered in the conversion from gate voltage V_G to pinch-off V_P in EKV 2.6. If the channel is short, the extension of space charge region from drain to the channel will weaken the controllability of gate voltage, resulting in the threshold lowering, shown in Fig. 2. [1] On the contrary, gate voltage tends to control more charge from the lateral side of the channel for a narrow channel, leading to a larger threshold, shown in Fig. 3. [1]

4) Reverse short channel effect: To combat drain-induced barrier lowering (DIBL), the channel of transistor near drain and source terminal tends to be more doped. For a short channel, the heavily doping area of source will overlap that

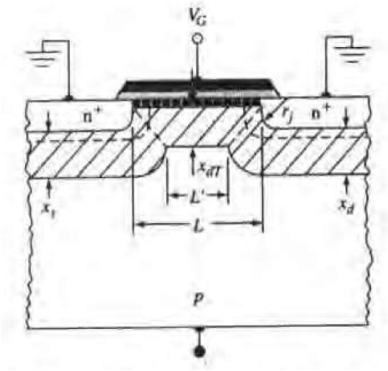

Fig. 2. Short channel charge sharing

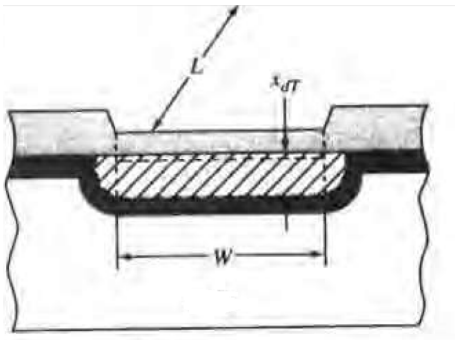

Fig. 3. Narrow channel charge sharing

of drain, increasing the average concentration of the channel, thus increasing the threshold voltage. [11] This effect is taken account of in the gate voltage calculation in EKV 2.6.

5) Mobility effects due to vertical fields: Carriers tend to be attracted by the vertical electric field in the channel, moving towards the surface of the channel, and then due to the accumulation of carriers, the Coulomb force will push the carriers away from the surface. This effect is called surface scattering, shown in Fig. 4, which lengthen the moving distance of carriers, equivalently reducing the mobility to some extent. [1] The effect is directly modified on mobility μ in EKV 2.6 model.

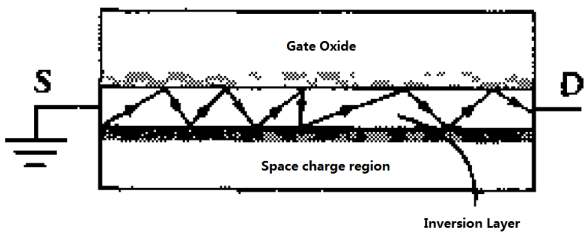

Fig. 4. The carrier moving trace in inversion layer

III. Software Implementation

This tool realize a software with GUI simulating one transistor performance applying EKV 2.6 model. The tool include an model engine calculating all parameter of the transistor. Due to the lack of process parameter, only two secondary effects: channel length modulation and velocity saturation are included in the engine. The small signal element like g_m, g_{mb}, g_{ds} are also extracted by hard-code inside the engine. The

The Newton-Raphson algorithm for calculation normalized mobile charge density q from pinch-off V_P in [12] is improved. According to Equation 1, the iterative function can be obtained below.

$$q^{(n+1)} = q^{(n)} - \frac{f\left(q^{(n)}\right)}{f'\left(q^{(n)}\right)} = q^{(n)} - \frac{2q^{(n)} + \ln\left(q^{(n)}\right) + C}{2 + 1/q^{(n)}} \quad (4)$$

In the equation above, C is a value determine by bias voltage, thus q is calculated iteratively for a given V_P. If the q becomes a negative value, the iteration will be stopped since logarithm function doesn't accept negative variable. The original solution for this is set a positive constant small value q_+ when negative q comes out. [12] However, this method may cause the situation that q may stick at a loop, and never converge when calculation some reverse inversion level i_r. The new solution for this is replacing the constant value q_+ with a value that reduce by decade each time detecting a negative q occurring. This solution can get more q solution than the original one in the same convergence constraint. Another solution is substitute the exponential function for logarithm one, which may avoid the negative q problem, but inducing more possibility for inaccuracy.

Figure 5 shows the GUI of the software. On the left side, user are allowed to adjust the size and voltage bias for the transistor, and the large-signal and small-signal performance of it is listed below. On the right side, a region for plotting is shown, enabling automatically plot the curve like I_{ds} vs. V_{ds}, g_m vs. I_d. Several curves are allowed to be kept for comparison, or removing some curves is supported, as well. The tool can also export the performance or plot data for specific transistor into a file. All the process parameter used now for the engine is extracted from some specific value from TSMC 0.18um process except λ for channel length modulation.

IV. Simulation Results and Discussion

Since g_m/I_{ds} methodology depends on the g_m/I_{ds} curve to a great extent, which is also a representative performance of EKV model. The two test circuits are designed for the simulation, shown in Fig. 6. The test circuit with voltage bias (Fig. 6(a)) sets drain voltage to $1.8V$, and sweep gate voltage to get the drain current and transconductance. The test circuit with current bias (Fig. 6(b)) directly sweep the drain current in a linear selection for points to obtain the transconductance. The test results are almost the same, however, the second is much convenient for simulation, thus all the test below apply the second test circuit.

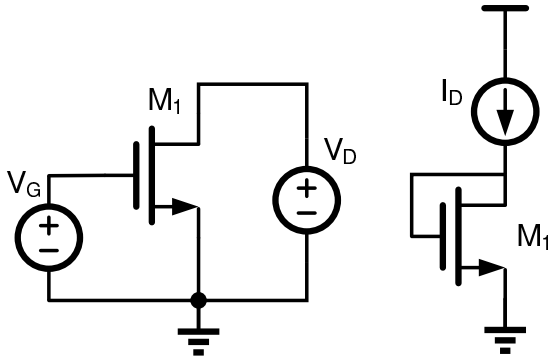

(a) Voltage Bias (b) Current Bias

Fig. 6. Test Circuits

Simulation in Cadence SpectreRF with BSIM model is first simulated. The g_m/I_d curve of NMOS and PMOS are depicted in Fig. 7, which shows a great divergence on the magnitude of the curves due to the mobility difference.

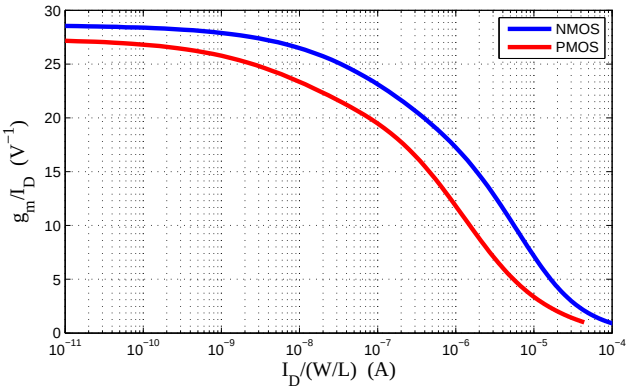

Fig. 7. g_m/I_D Curve of NMOS and PMOS transistor

To verify the stability of the g_m/I_d curve [9], several channel lengths L with the same aspect ratio are selected. The result is shown in Fig. 8, denouncing the correctness of stability in weak inversion, which is shown in [13], as well. Since the x axis is in log scale, which means the fact that a slight difference in curve may cause a big sizing fault. Therefore an accurate CAD tool to reveal this phenomenon is required urgently.

The equation for g_m/I_d is given in [7], shown as follows:

$$\frac{g_m}{I_d} \approx \frac{1}{nV_T\left(\sqrt{IC + 0.25} + 0.5\right)} \approx \frac{1 - \exp -\sqrt{IC}}{nV_T\sqrt{IC}} \quad (5)$$

Fitting is processed for both forms of g_m/I_d in Equation 5. The results of fitting are illustrated in Fig. 9 and Fig. 10. The root mean square error for the two fit curves are 0.2336 and 0.1953, which is relatively large and significant error can be seen on the figures.

The reason for large error in fitting is suspected that BSIM model doesn't model the performance of transistor in weak

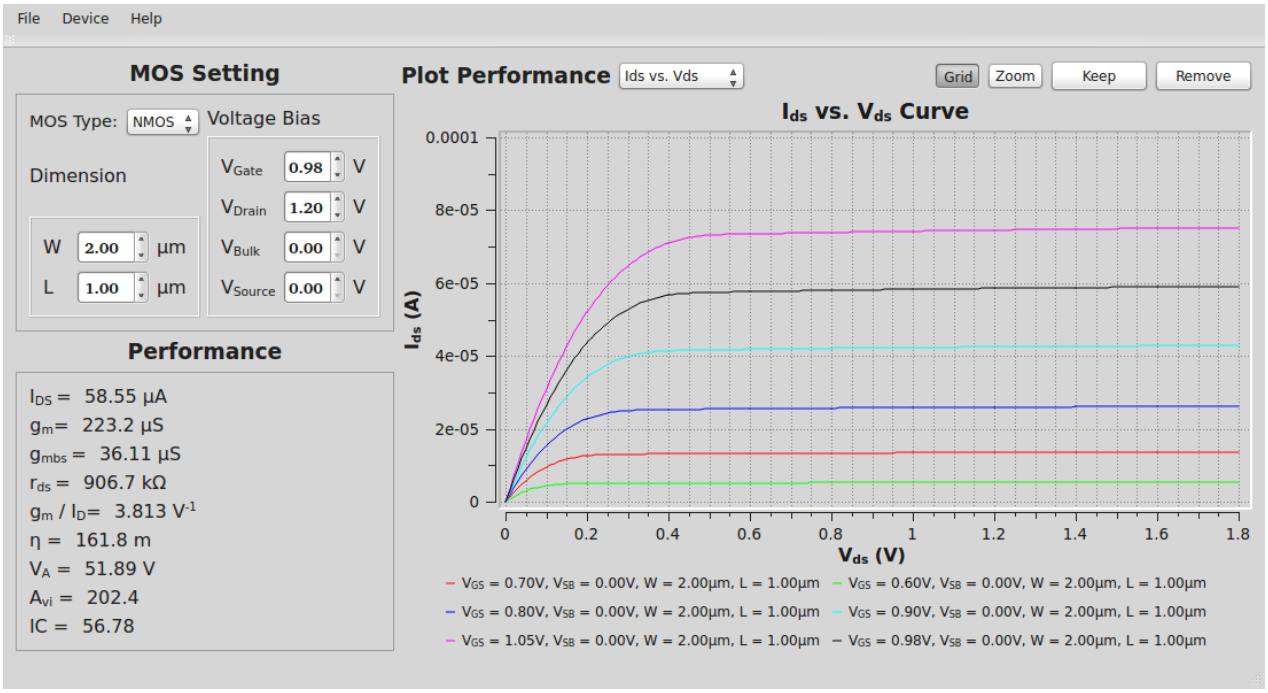

Fig. 5. The graphical user interface of software

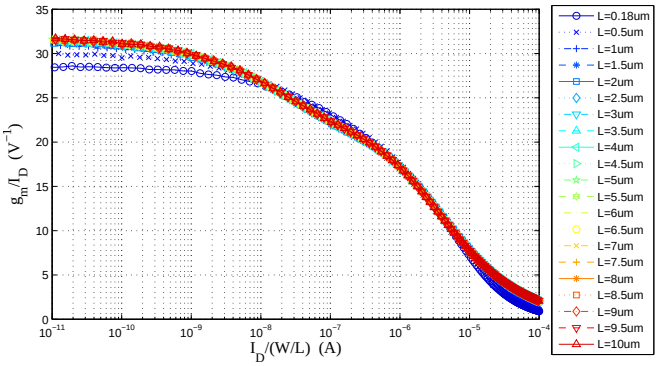

Fig. 8. g_m/I_D Curve of NMOS transistors with different value for L

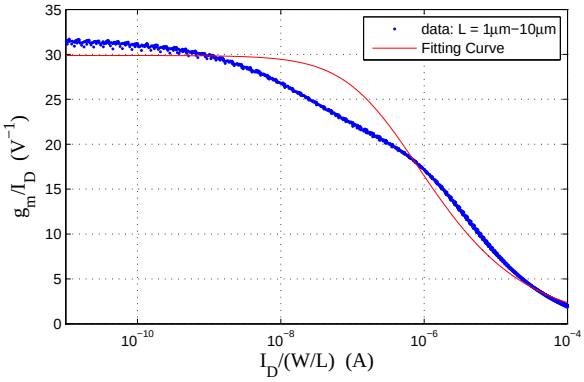

Fig. 9. Fitting curve of $\frac{1}{nV_T(\sqrt{IC}+0.25+0.5)}$

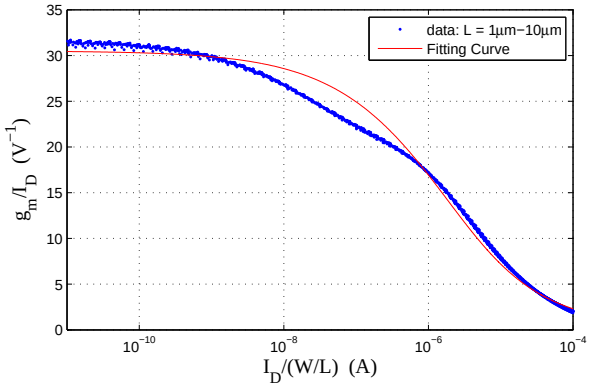

Fig. 10. Fitting curve of $\frac{1-\exp-\sqrt{IC}}{nV_T\sqrt{IC}}$

or moderate inversion accurately. For the fitting curve, it is larger than the simulation data in weak and moderate inversion, which is also shown in [14], and the EKV curve is more approximate the real measured curve.

Then the simulation is taken under simple EKV model [12] and EKV 2.6 model. The comparison of g_m/I_D curve between simple EKV model and proposed one is shown in the Fig. 11. The reason of large divergence in weak and moderate inversion is still unknown.

The channel length modulation for simple EKV model is given in Fig. 12.

It can be seen that the CLM doesn't have any effect on the weak or moderate inversion, but only occurs in strong inversion, since the saturation region is specialized like what is induced in square law model, which may cause the dis-

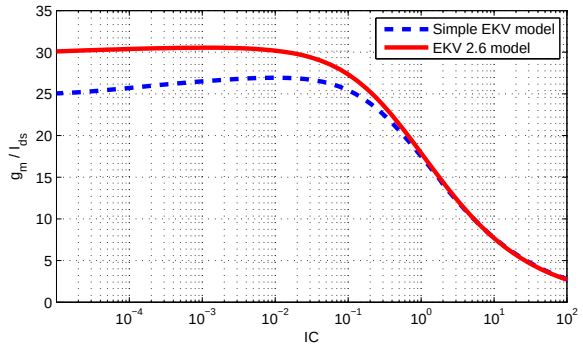

Fig. 11. Comparison of g_m/I_D between Chen's model and proposed one

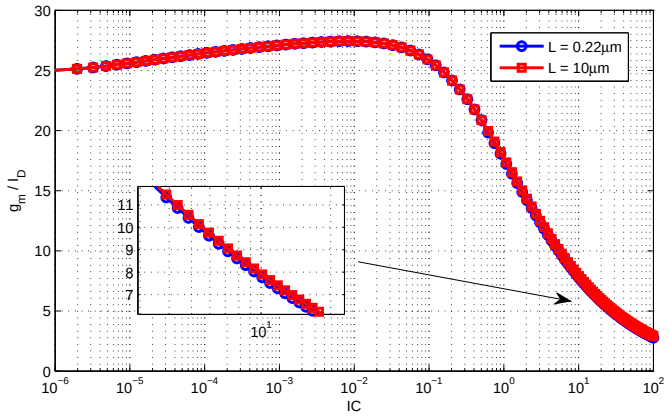

Fig. 12. Channel length Modulation in simple EKV model

continuity of the derivation of the some parameter, leading to convergence problem when modified nodal analysis(MNA) method is applied. The same curve for EKV 2.6 model considering channel length modulation and velocity saturation is shown in Fig. 13.

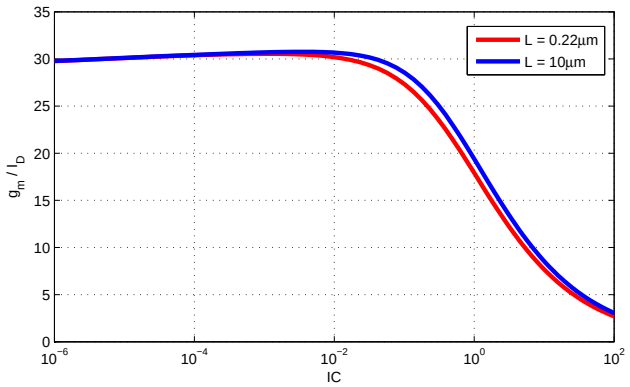

Fig. 13. Channel length Modulation in EKV 2.6 model

It can be seen both simple EKV model and EKV 2.6 always converge to the same value in weak conversion. However, simulated in [14], even EKV model can model this effect due to the adjustment of channel length L. The plan for improving this is taking account into more secondary effects in our CAD tool, since both second-order effects considered now occurs in strong inversion. However, the process parameter will be another obstacle.

V. Conclusion

This article illustrates the basic EKV model and explain several secondary effects considered in EKV 2.6 model. A CAD tool with GUI implemented with an engine simulating EKV 2.6 model is given. Several simulation results are given and discussed, showing that current EKV model realized still need to consider more effects to cater the requirement of g_m/I_D methodology.

Appendix

All the equation used in the MOS performance calculation engine is summarized here for record. [8]

A. Constant physical value calculation

The value taken from the standard TSMC $0.18\mu m$ process are listed in Table I.

TABLE I
Process Parameter

Description	Symbol
Channel doping concentration	N_{ch}
Oxide thickness	t_{ox}
Threshold voltage	V_{th0}
Carrier mobility	μ
Junction depth	x_j
Saturation velocity	υ_{sat}
Depletion length coefficient	λ

λ for channel length modulation is set 0.5 according to [15]. The value for some physical constant is listed on following Table II.

TABLE II
Physical Parameter

Description	Value
Permittivity of silicon	$\epsilon_{si} = 104.5 \times 10^{-12} F/m$
Permittivity of silicon dioxide	$\epsilon_{ox} = 34.5 \times 10^{-12} F/m$
Magnitude of electron charge	$Q = 1.602 \times 10^{-19} C$
Boltzmann constant	$k = 1.3807 \times 10^{-23} JK^{-1}$
Reference Temperature	$T_{ref} = 300.15K$
Intrinsic carrier concentration	$n_i = 1.45 \times 10^{10} cm^{-3}$

The equation for parameter applied in EKV 2.6 model is listed in Table III.

B. Voltage setting

Voltages are all referred to the local substrate. For P-channel devices, all sign of the below voltages are inverted.

$$V_G = V_{GB} = V_{GS} - V_{BS} \quad (6)$$

$$V_S = V_{SB} = -V_{BS} \quad (7)$$

$$V_D = V_{DB} = V_{DS} - V_{BS} \quad (8)$$

TABLE III
PHYSICAL PARAMETER

Description	Equation
Thermal voltage	$V_T = \frac{kT_{ref}}{Q}$
Unit gate oxide capacitance	$C_{ox} = \frac{\epsilon_{ox}}{t_{ox}}$
Bulk Fermi potential	$\psi = 2V_T \ln\left(\frac{N_{ch}}{n_i}\right)$
Body effect parameter	$\gamma = \frac{\sqrt{2Q\epsilon_{si}N_{ch} \times 10^6}}{C_{ox}}$
Mobility parameter	$k^{'} = \mu C_{ox}$
Saturation electric field	$E_{sat} = \frac{v_{sat}}{\mu}$

C. Pinch-off voltage

Pinch-off voltage is calculated as below.

$$V_G^{'} = V_G - V_{th0} + \psi + \gamma\sqrt{\psi} \tag{9}$$

$$V_P = \begin{cases} V_G^{'} - \psi - \gamma\left(\sqrt{V_G^{'} + \left(\frac{\gamma}{2}\right)^2} - \frac{\gamma}{2}\right) & V_G^{'} > 0 \\ -\psi & V_G^{'} \leq 0 \end{cases} \tag{10}$$

In addition, the slope factor can be obtained by the equation below.

$$n = 1 + \frac{\gamma}{2\sqrt{V_P + \psi + 4V_T}} \tag{11}$$

D. Inversion coefficient

The inversion coefficient is determined by a Newton-Raphson iteration, shown in Equation 4. The C is the input of the algorithm, thus the normalized mobile charge density q is determined by the formula below.

$$q = invq\left(\frac{V_P - V}{V_T}\right) \tag{12}$$

Setting V as V_S and V_D, the corresponding q_f and q_r can be calculated, and then the inversion level of forward current and reverse one can be derived from the formula below, as well as the inversion level IC.

$$i_f = q_f^2 + q_f \quad i_r = q_r^2 + q_r \tag{13}$$

$$IC = i_f - i_r \tag{14}$$

E. Secondary effect calculation

The channel length modulation and velocity saturation are included in the following equation.

$$V_C = E_{sat}L \tag{15}$$

$$V_{DSS} = V_C\left(\sqrt{\frac{1}{4} + \frac{V_T}{V_C}\sqrt{i_f}} - \frac{1}{2}\right) \tag{16}$$

$$\Delta V = 4V_T\sqrt{\lambda\left(\sqrt{i_f} - \frac{V_{DSS}}{V_T}\right) + \frac{1}{64}} \tag{17}$$

$$V_{ds} = \frac{V_D - V_S}{2} \tag{18}$$

$$V_{ip} = \sqrt{{V_{DSS}}^2 + \Delta V^2} - \sqrt{\left(V_{ds} - V_{DSS}\right)^2 + \Delta V^2} \tag{19}$$

$$L_C = \sqrt{\frac{\epsilon_{si}}{C_{ox}}x_j} \tag{20}$$

$$\Delta L = \lambda L_C \ln\left(1 + \frac{V_{ds} - V_{ip}}{L_C E_{sat}}\right) \tag{21}$$

$$L^{'} = L - \Delta L + \frac{V_{ds} - V_{ip}}{E_{sat}} \tag{22}$$

$$L_{min} = \frac{L}{10} \tag{23}$$

$$L_{eq} = \frac{1}{2}\left(L^{'} + \sqrt{{L^{'}}^2 + {L_{min}}^2}\right) \tag{24}$$

F. Drain current

For given equivalent channel length, β is easily calculated, and the drain current of the transistor can be given as follows.

$$\beta = k^{'}\frac{W}{L_{eq}} \tag{25}$$

$$I_N = 2n\beta V_T^2 \tag{26}$$

$$I_{ds} = I_N IC \tag{27}$$

G. Small-signal definition

The transconductance are obtained through derivation of the drain current:

$$g_{mg} \equiv \frac{\partial I_{ds}}{\partial V_G} \quad g_{ms} \equiv -\frac{\partial I_{ds}}{\partial V_S} \quad g_{md} \equiv \frac{\partial I_{ds}}{\partial V_D} \tag{28}$$

Then the traditional small-signal parameter can be calculated as follows:

$$g_m \equiv \frac{\partial I_{ds}}{\partial V_{GS}} = g_{mg} \tag{29}$$

$$g_{mbs} \equiv \frac{\partial I_{ds}}{\partial V_{BS}} = g_{ms} - g_{mg} - g_{md} \tag{30}$$

$$g_{ds} \equiv \frac{\partial I_{ds}}{\partial V_{DS}} = g_{md} \tag{31}$$

H. Small-signal g_{mg}

The small-signal transconductance g_{mg} is calculated as follows.

$$\frac{\partial V_P}{\partial V_G} = \frac{\partial V_P}{\partial V'_G}\frac{\partial V'_G}{\partial V_G} = \frac{\partial V_P}{\partial V'_G} = 1 - \frac{\gamma}{\sqrt{4V'_G + \gamma^2}} \quad (32)$$

$$\frac{\partial i_{f,r}}{\partial V_G} = \frac{\partial i_{f,r}}{\partial q_{f,r}}\frac{\partial q_{f,r}}{\partial V_G} = (2q_{f,r}+1)\frac{\partial q_{f,r}}{\partial V_P}\frac{\partial V_P}{\partial V_G}$$
$$= (2q_{f,r}+1)\frac{q_{f,r}}{(2q_{f,r}+1)V_T}\frac{\partial V_P}{\partial V_G}$$
$$= \frac{q_{f,r}}{V_T}\frac{\partial V_P}{\partial V_G} \quad (33)$$

$$\frac{\partial n}{\partial V_G} = \frac{\partial n}{\partial V_P}\frac{\partial V_P}{\partial V_G}$$
$$= -\frac{\gamma}{4}\left(V_P + \Phi + 4V_T\right)^{-\frac{3}{2}}\frac{\partial V_P}{\partial V_G} \quad (34)$$

$$\frac{\partial V_{DSS}}{\partial V_G} = \frac{V_C V_T}{2V_{DSS}+V_C}\frac{1}{2\sqrt{i_f}}\frac{\partial i_f}{\partial V_G} \quad (35)$$

$$\frac{\partial \Delta V}{\partial V_G} = \frac{8\lambda V_T^2}{\Delta V}\left(\frac{1}{2\sqrt{i_f}}\frac{\partial i_f}{\partial V_G} - \frac{1}{V_T}\frac{\partial V_{DSS}}{\partial V_G}\right) \quad (36)$$

$$\frac{\partial V_{ip}}{\partial V_G} = \frac{V_{DSS}\frac{\partial V_{DSS}}{\partial V_G} + \Delta V\frac{\partial \Delta V}{\partial V_G}}{\sqrt{V_{DSS}^2 + \Delta V^2}}$$
$$- \frac{\Delta V\frac{\partial \Delta V}{\partial V_G} - (V_{ds}-V_{DSS})\frac{\partial V_{DSS}}{\partial V_G}}{\sqrt{(V_{ds}-V_{DSS})^2 + \Delta V^2}} \quad (37)$$

$$\frac{\partial \Delta L}{\partial V_G} = \frac{\partial \Delta L}{\partial V_{ip}}\frac{\partial V_{ip}}{\partial V_G}$$
$$= \frac{\lambda L_C}{V_{ip}-V_{ds}-L_C E_{sat}}\frac{\partial V_{ip}}{\partial V_G} \quad (38)$$

$$\frac{\partial L'}{\partial V_G} = \frac{1}{E_{sat}}\left(\frac{\partial V_{ds}}{\partial V_G} + \frac{\partial V_{ip}}{\partial V_G}\right) - \frac{\partial \Delta L}{\partial V_G}$$
$$= \frac{1}{E_{sat}}\frac{\partial V_{ip}}{\partial V_G} - \frac{\partial \Delta L}{\partial V_G} \quad (39)$$

$$\frac{\partial L_{eq}}{\partial V_G} = \frac{\partial L_{eq}}{\partial L'}\frac{\partial L'}{\partial V_G}$$
$$= \frac{1}{2}\left(1 + \frac{L'}{\sqrt{L'^2 + L_{min}^2}}\right)\frac{\partial L'}{\partial V_G} \quad (40)$$

$$\frac{\partial \beta}{\partial V_G} = \frac{\partial \beta}{\partial L_{eq}}\frac{\partial L_{eq}}{\partial V_G} = -k'\frac{W}{L_{eq}^2}\frac{\partial L_{eq}}{\partial V_G} \quad (41)$$

$$\frac{\partial I_N}{\partial V_G} = 2V_T^2\left(\beta\frac{\partial n}{\partial V_G} + n\frac{\partial \beta}{\partial V_G}\right) \quad (42)$$

$$g_{mg} = \frac{\partial I_{ds}}{\partial V_G} = (i_f - i_r)\frac{\partial I_N}{\partial V_G} + I_N\frac{\partial (i_f - i_r)}{\partial V_G}$$
$$= IC\frac{\partial I_N}{\partial V_G} + I_N\left(\frac{\partial i_f}{\partial V_G} - \frac{\partial i_r}{\partial V_G}\right) \quad (43)$$

I. Small-signal g_{ms}

The small-signal transconductance g_{ms} is calculated as follows.

$$\frac{\partial i_f}{\partial V_S} = \frac{\partial i_f}{\partial q_f}\frac{\partial q_f}{\partial V_S} = (2q_f+1)\frac{\partial q_f}{\partial V_P}\frac{\partial V_P}{\partial V_S}$$
$$= -\frac{q_f}{V_T} \quad (44)$$

$$\frac{\partial V_{DSS}}{\partial V_S} = \frac{V_C V_T}{2V_{DSS}+V_C}\frac{1}{2\sqrt{i_f}}\frac{\partial i_f}{\partial V_S} \quad (45)$$

$$\frac{\partial \Delta V}{\partial V_S} = \frac{8\lambda V_T^2}{\Delta V}\left(\frac{1}{2\sqrt{i_f}}\frac{\partial i_f}{\partial V_S} - \frac{1}{V_T}\frac{\partial V_{DSS}}{\partial V_S}\right) \quad (46)$$

$$\frac{\partial V_{ip}}{\partial V_S} = \frac{V_{DSS}\frac{\partial V_{DSS}}{\partial V_S} + \Delta V\frac{\partial \Delta V}{\partial V_S}}{\sqrt{V_{DSS}^2 + \Delta V^2}}$$
$$- \frac{\Delta V\frac{\partial \Delta V}{\partial V_S} - (V_{ds}-V_{DSS})\left(\frac{\partial V_{DSS}}{\partial V_S} + \frac{1}{2}\right)}{\sqrt{(V_{ds}-V_{DSS})^2 + \Delta V^2}} \quad (47)$$

$$\frac{\partial \Delta L}{\partial V_S} = \frac{\lambda L_C}{V_{ip}-V_{ds}-L_C E_{sat}}\left(\frac{1}{2} + \frac{\partial V_{ip}}{\partial V_D}\right) \quad (48)$$

$$\frac{\partial L'}{\partial V_S} = \frac{1}{E_{sat}}\left(\frac{\partial V_{ds}}{\partial V_S} + \frac{\partial V_{ip}}{\partial V_S}\right) - \frac{\partial \Delta L}{\partial V_S}$$
$$= \frac{1}{E_{sat}}\left(\frac{\partial V_{ip}}{\partial V_S} - \frac{1}{2}\right) - \frac{\partial \Delta L}{\partial V_S} \quad (49)$$

$$\frac{\partial L_{eq}}{\partial V_S} = \frac{1}{2}\left(1 + \frac{L'}{\sqrt{L'^2 + L_{min}^2}}\right)\frac{\partial L'}{\partial V_S} \quad (50)$$

$$\frac{\partial \beta}{\partial V_S} = -\frac{k'W}{L_{eq}^2}\frac{\partial L_{eq}}{\partial V_S} \quad (51)$$

$$\frac{\partial I_N}{\partial V_S} = 2nV_T^2\frac{\partial \beta}{\partial V_S} \quad (52)$$

$$g_{ms} = -\frac{\partial I_{ds}}{\partial V_S} = -\left(IC\frac{\partial I_N}{\partial V_S} + I_N\frac{\partial i_f}{\partial V_S}\right) \quad (53)$$

J. Small-signal g_{md}

The small-signal transconductance g_{md} is calculated as follows.

$$\frac{\partial i_r}{\partial V_D} = \frac{\partial i_r}{\partial q_r}\frac{\partial q_r}{\partial V_D} = (2q_r+1)\frac{\partial q_r}{\partial V_P}\frac{\partial V_P}{\partial V_D}$$
$$= -\frac{q_r}{V_T} \quad (54)$$

$$\frac{\partial V_{ip}}{\partial V_D} = \frac{V_{DSS}-V_{ds}}{2\sqrt{(V_{DSS}-V_{ds})^2 + \Delta V^2}} \quad (55)$$

$$\frac{\partial \Delta L}{\partial V_D} = \frac{\lambda L_C}{L_C E_{sat} + V_{ds} - V_{ip}}\left(\frac{1}{2} - \frac{\partial V_{ip}}{\partial V_D}\right) \quad (56)$$

$$\frac{\partial L'}{\partial V_D} = \frac{1}{E_{sat}}\left(\frac{\partial V_{ip}}{\partial V_D} + \frac{1}{2}\right) - \frac{\partial \Delta L}{\partial V_D} \quad (57)$$

$$\frac{\partial L_{eq}}{\partial V_D} = \frac{1}{2}\left(1 + \frac{L'}{\sqrt{L'^2 + L_{min}^2}}\right)\frac{\partial L'}{\partial V_D} \quad (58)$$

$$\frac{\partial \beta}{\partial V_D} = -\frac{k'W}{L_{eq}^2}\frac{\partial L_{eq}}{\partial V_D} \quad (59)$$

$$\frac{\partial I_N}{\partial V_D} = 2nV_T^2\frac{\partial \beta}{\partial V_D} \quad (60)$$

$$g_{md} = \frac{\partial I_{ds}}{\partial V_D} = IC\frac{\partial I_N}{\partial V_D} - I_N\frac{\partial i_r}{\partial V_D} \quad (61)$$

K. Quasi-static intrinsic elements

The simplified capacitive dynamic model of normalized intrinsic capacitances can be obtained below.

$$n_q = 1 + \frac{\gamma}{2\sqrt{V_P + \phi + 10^{-6}}} \quad (62)$$

$$x_f = \sqrt{\frac{1}{4} + i_f} \quad (63)$$

$$x_r = \sqrt{\frac{1}{4} + i_r} \quad (64)$$

$$c_{gs} = \frac{2}{3}\left(1 - \frac{x_r^2 + x_r + \frac{1}{2}x_f}{(x_f + x_r)^2}\right) \quad (65)$$

$$c_{gd} = \frac{2}{3}\left(1 - \frac{x_f^2 + x_f + \frac{1}{2}x_r}{(x_f + x_r)^2}\right) \quad (66)$$

$$c_{gb} = \frac{n_q - 1}{n_q}(1 - c_{gs} - c_{gd}) \quad (67)$$

$$c_{sb} = (n_q - 1)\, c_{gs} \quad (68)$$

$$c_{db} = (n_q - 1)\, c_{gd} \quad (69)$$

The corresponding total intrinsic capacitances is determined by:

$$C_{(gs,gd,gb,sb,db)} = C_{ox}WL \cdot c_{(gs,gd,gb,sb,db)} \quad (70)$$

L. Geometry capacitance

The geometry capacitance are mainly composed of two parts: overlapping capacitance C_{ov} between gate and diffusion region under the channel; junction capacitance C_{j0} around the diffusion region.

$$C_{ov} = c_{ov}W \quad (71)$$

$$C_{j0} = c_j L_S W + c_{jsw}(2L_S + W) \quad (72)$$

The L_S above depicts the length of diffusion region, and c_{ov} is the unit capacitance per unit length, and c_j and c_{jsw} represent the unit junction and side wall capacitance, respectively.

M. Others

Some extra performance is calculated as follows:

$$\eta = \frac{g_{mbs}}{g_m} \quad (73)$$

$$A_{vi} = \frac{g_m}{g_{ds}} \quad (74)$$

$$V_A = \frac{I_{ds}}{g_{ds}} - (V_D - V_S)\,; \quad (75)$$

η is the ratio between g_m and g_{mbs}, A_{vi} is the intrinsic gain of the transistor, and V_A is the Early voltage.

REFERENCES

[1] D. A. Neamen and B. Pevzner, *Semiconductor physics and devices: basic principles*. McGraw-Hill New York, 2003, vol. 3.

[2] J. Brews, "A charge-sheet model of the mosfet," *Solid-State Electronics*, vol. 21, no. 2, pp. 345–355, 1978.

[3] F. Van de Wiele, "A long-channel mosfet model," *Solid-State Electronics*, vol. 22, no. 12, pp. 991–997, 1979.

[4] C. C. Enz, F. Krummenacher, and E. A. Vittoz, "An analytical mos transistor model valid in all regions of operation and dedicated to low-voltage and low-current applications," *Analog integrated circuits and signal processing*, vol. 8, no. 1, pp. 83–114, 1995.

[5] F. Silveira, D. Flandre, and P. G. A. Jespers, "A g_m/I_D based methodology for the design of cmos analog circuits and its application to the synthesis of a silicon-on-insulator micropower ota," *Solid-State Circuits, IEEE Journal of*, vol. 31, no. 9, pp. 1314–1319, 1996.

[6] P. G. Jespers, *The g_m/I_D Design Methodology, a Sizing Tool for Low-voltage Analog CMOS Circuits: The Semi-empirical and Compact Model Approaches*. Springer, 2010, vol. 29.

[7] D. Binkley, C. Hopper, S. D. Tucker, B. C. Moss, J. Rochelle, and D. Foty, "A cad methodology for optimizing transistor current and sizing in analog cmos design," *Computer-Aided Design of Integrated Circuits and Systems, IEEE Transactions on*, vol. 22, no. 2, pp. 225–237, 2003.

[8] M. Bucher, C. Lallement, C. Enz, F. Théodoloz, and F. Krummenacher, "The epfl-ekv mosfet model equations for simulation," *Eletronics Laboratories (LEG), Swiss Federal Institute of Technology (EPFL), Lausanne, Switzerland*, 1997.

[9] D. Foty, M. Bucher, and D. Binkley, "Re-interpreting the mos transistor via the inversion coefficient and the continuum of g_{ms}/I_d," in *Electronics, Circuits and Systems, 2002. 9th International Conference on*, vol. 3, 2002, pp. 1179–1182.

[10] J. M. Rabaey, A. Chandrakasan, and B. Nikolic, *Digital integrated circuits*. Prentice Hall Upper Saddle River, NJ, 2003.

[11] Wikipedia, "Reverse short-channel effect," http://en.wikipedia.org/wiki/Reverse_short-channel_effect.

[12] J. Chen, G. Shi, A. Tai, and F. Lee, "A size sensitivity method for interactive mos circuit sizing," in *New Circuits and Systems Conference (NEWCAS), 2012 IEEE 10th International*, 2012, pp. 169–172.

[13] M. Bucher, A. Bazigos, and W. Grabinski, "Determining mosfet parameters in moderate inversion," in *Design and Diagnostics of Electronic Circuits and Systems, 2007. DDECS '07. IEEE*, 2007, pp. 1–4.

[14] S. Terry, J. Rochelle, D. Binkley, B. Blalock, D. Foty, and M. Bucher, "Comparison of a bsim3v3 and ekv mosfet model for a 0.5 μm cmos process and implications for analog circuit design," *Nuclear Science, IEEE Transactions on*, vol. 50, no. 4, pp. 915–920, 2003.

[15] EPFL, "180nm cmos parameters, ekv v301.01 indicative data," http://ekv.epfl.ch/page-44590-en.html.